Biochimica et Biophysica Acta 1838 (2014) 2547–2554

Contents lists available at ScienceDirect

Biochimica et Biophysica Acta

journal homepage: www.elsevier.com/locate/bbamem

Calcium-mediated pore expansion and cell death following nanoelectroporation

Olga N. Pakhomova *, Betsy Gregory, Iurii Semenov, Andrei G. Pakhomov

Frank Reidy Research Center for Bioelectrics, Old Dominion University, Norfolk, VA, USA

ARTICLE INFO

Article history:
Received 9 May 2014
Received in revised form 19 June 2014
Accepted 20 June 2014
Available online 28 June 2014

Keywords:
Nanosecond pulse
Electroporation
Electropermeabilization
Calcium
Necrosis
Apoptosis

ABSTRACT

Opening of long-lived pores in the cell membrane is the principal primary effect of intense, nanosecond pulsed electric field (nsPEF). Here we demonstrate that the evolution of pores, cell survival, the time and the mode of cell death (necrotic or apoptotic) are determined by the level of external Ca^{2+} after nsPEF. We also introduce a novel, minimally disruptive technique for nsEP exposure of adherent cells on indium tin oxide (ITO)-coated glass coverslips, which does not require cell detachment and enables fast exchanges of bath media. Increasing the Ca^{2+} level from the nominal 2–5 μM to 2 mM for the first 60–90 min after permeabilization by 300-nsPEF increased the early (necrotic) death in U937, CHO, and BPAE cells. With nominal Ca^{2+}, the inhibition of osmotic swelling rescued cells from the early necrosis and increased caspase 3/7 activation later on. However, the inhibition of swelling had a modest or no protective effect with 2 mM Ca^{2+} in the medium. With the nominal Ca^{2+}, most cells displayed gradual increase in YO-PRO-1 and propidium (Pr) uptake. With 2 mM Ca^{2+}, the initially lower Pr uptake was eventually replaced by a massive and abrupt Pr entry (necrotic death). It was accompanied by a transient acceleration of the growth of membrane blebs due to the increase of the intracellular osmotic pressure. We conclude that the high-Ca^{2+}-dependent necrotic death in nsPEF-treated cells is effected by a delayed, sudden, and osmotically-independent pore expansion (or de novo formation of larger pores), but not by the membrane rupture.

1. Introduction

Effects of intense nsPEF treatments in mammalian cells include permeabilization of the plasma membrane, endoplasmic reticulum (ER), and mitochondria [1–7]; Ca^{2+} uptake from the outside and release from the ER [2,6,8–10]; destruction of the cytoskeleton [11–13]; cell swelling and blebbing [14–16]; and activation of signaling and cell death pathways [10,17–21]. The cytotoxic effects of nsPEF have attracted particular attention as a novel and promising modality for cancer treatment [22–26].

With the complexity of the cellular response to nsPEF, the mechanisms and specific pathways leading to cell death have only been partially understood. The early studies focused on the apoptotic response, and only recently early necrosis was reported by several groups as a separate or even a predominant mode of nsPEF-induced cell death [15,18]. The primary cause of necrosis was the persistent plasma membrane permeabilization to small solutes (<1 nm), which resulted in the osmotic imbalance, water uptake, and cell swelling culminating in the membrane rupture. When the uptake of water was blocked by an isoosmotic addition of a pore-impermeable solute (sucrose [14]), cells were rescued from the necrotic death, but nonetheless died later on by apoptosis [15]. However, the cause of the apoptosis in cells rescued from the necrosis was not identified.

Ca^{2+} signaling is critically involved, in many ways, in both the initiation and effectuation of the cell death (see [27] for review). Several studies pointed to the role of mitochondria and Ca^{2+} increase in the initiation and execution of the nsPEF-induced apoptosis [3,28], and the increase in the cytosolic Ca^{2+} is one of the best known nsPEF effects [2,6,8,9,29,30]. In human pancreatic cancer cells, nsPEF caused Ca^{2+}-dependent production of reactive oxygen species, indicating that overloading mitochondria with Ca^{2+} and their destruction were part of the apoptotic mechanism [28]. Finally, cell lethality increased with increasing extracellular Ca^{2+} for either nsPEF or conventional electroporation [31,32]. The injection of Ca^{2+} into a tumor prior to its electroablation ("Ca^{2+} electroporation") has increased the treatment efficiency in animals and humans [31].

Abbreviations: BPAE, bovine pulmonary artery endothelial cells; ER, endoplasmic reticulum; nsPEF, nanosecond pulsed electric field; Pr, propidium; ROS, reactive oxygen species

* Corresponding author at: Frank Reidy Research Center for Bioelectrics, 4211 Monarch Way, Suite 300, Old Dominion University, Norfolk, VA 23508, USA. Tel.: +1 210 6182824, +1 757 6838006; fax: +1 757 4511010.
E-mail addresses: opakhomo@odu.edu, olga@pakhomova.net (O.N. Pakhomova).

http://dx.doi.org/10.1016/j.bbamem.2014.06.015
0005-2736/

Therefore, our experiments were initially aimed at defining the role of Ca^{2+} in nsPEF-induced apoptosis in cells rescued from the early osmotically-driven necrosis. Instead, we found that the increased Ca^{2+} facilitated the early necrosis and thereby decreased the cell population that could potentially enter the apoptotic process. The Ca^{2+}-mediated necrotic pathway did not rely on the osmotic swelling, and overrode any protection rendered by the blockage of water uptake. Below we demonstrate that Ca^{2+}-mediated necrosis results from a delayed, abrupt, irreversible, and osmotically-independent expansion of pores in the cell membrane.

2. Materials and methods

2.1. Cells and media

We utilized suspension cells U937 (human monocytes), and adherent cells CHO-K1 (Chinese hamster ovary) and BPAE (bovine pulmonary artery endothelial). U937 and CHO cells were obtained from the American Type Culture Collection (ATCC, Manassas, VA) and propagated as described previously [1,15,33]. BPAE were a kind gift from Dr. J. Catravas (Center for Bioelectrics, ODU). They were grown at 37 °C with 5% CO_2 in air in a low glucose DMEM with 10% fetal bovine serum (FBS), 100 IU/ml penicillin, 0.1 mg/ml streptomycin, and 2.5 μg/ml amphotericin B. The media and its components were purchased from Thermo Scientific (Waltham, MA), Sigma-Aldrich (St. Louis, MO), and Atlanta Biologicals (Norcross, GA).

2.2. nsPEF exposure and viability of suspension cells

To control for the extracellular Ca^{2+} during and after nsPEF, we utilized RPMI 1640 medium formulated without Ca^{2+} ("no Ca^{2+}" medium). Ca^{2+} chelators were not used, as their possible entry into electropermeabilized cells could affect the cytosolic free Ca^{2+} level and the physiological consequences of electroporation. The actual level of free Ca^{2+} in this medium was checked by ratiometric fluorescence with Fura-2 [2] and equaled 1–2 μM.

U937 cells were spun and rinsed twice, resuspended in no Ca^{2+} RPMI at 3×10^6 cells/ml, and then split into two aliquots. In one of them, Ca^{2+} level was raised to 2 mM ("2 Ca^{2+}" medium).

The samples were transferred into 1-mm gap electroporation cuvettes and exposed to 300 pulses of 300-ns duration, at 700 V amplitude and 10 Hz repetition rate from an AVTECH AVOZ-D2-B-ODA generator (AVTECH Electrosystems, Ottawa, Canada) as described earlier [15,33]. Parallel controls were "sham" exposed. Immediately following either nsPEF or sham treatment, all samples were mixed with a 6× volume of the same medium (0Ca^{2+} or 2Ca^{2+}) and a 3× volume of an isoosmotic (290 mOsm/kg) water solution of either sucrose or NaCl [15]. As a nanopore-impermeable solute, sucrose was shown to prevent the osmotic water uptake in nsPEF-treated cells [14,15], thereby rescuing them from the osmotically-mediated necrosis. [15]. NaCl did not render such protection and served as a control for the equivalent dilution of the medium [15].

The samples in tested media (no Ca^{2+} + sucrose; no Ca^{2+} + NaCl; 2 Ca^{2+} + sucrose; and 2 Ca^{2+} + NaCl) were aliquoted into a 96-well plate at 100 μl/well and incubated at 37 °C for 1 h. This time interval was chosen to allow either for electropore resealing, or for cell rupture due to the osmotic imbalance if (most) pores failed to reseal. Next, all samples were supplemented with 10 μl of FBS and 10 μl of RPMI properly enriched with Ca^{2+}, in order to bring the Ca^{2+} level in all samples to 2 mM.

At 1.5, 4, or 24 h after nsPEF, 10 μl of the Presto Blue reagent (Life Technologies, Grand Island, NY) were added to the wells. After 1 h of incubation at 37 °C with the reagent, the wells were scanned with a Synergy 2 microplate reader (BioTek, Winooski, VT), using excitation at 530 nm and detection at 590 nm.

2.3. Caspase 3/7 activity

We utilized a Caspase-Glo 3/7 Assay from Promega (Madison, WI) according to the manufacturer's instructions. The buffer compositions, exposure, and sample handling protocols were the same as described in the above Section 2.2. In 1.5, 4, or 24 h after nsPEF exposure, cells were aliquoted at 50 μl/well into a 96-well plate and 50 μl of Caspase-Glo 3/7 reagent was added. The luminescence was measured by the Synergy 2 reader after 40 min of incubation at room temperature.

2.4. A novel concept of nsPEF exposure of adherent cells: the use of indium tin oxide (ITO)-coated glass coverslips

Electroporation cuvettes are designed for cell suspensions, so adherent cells need to be removed from the substrate prior to nsPEF treatment. This step alters cell physiology and may affect the survival rate, along with the re-attachment after nsPEF. The greatest challenge is the replacement of media in electroporated cells, which are too fragile to be spun (that is why we use only media dilutions and avoid centrifugation in Section 2.2).

Here, we introduce a novel method of nsPEF exposure of adherent cells in electroporation cuvettes, which utilizes ITO-coated glass coverslips and is devoid of stressful cell handling. ITO is a biologically inert material which uniquely combines high electrical conductance with optical transparency. If cells grown on a "regular" glass coverslip are pulsed in a cuvette, the glass layer shields the cells from the E-field. However, the ITO layer cancels this protection, resulting in an efficient and uniform nsPEF exposure of cells over the entire coverslip surface. The method does not require detachment or reattachment of cells, and changes of media are accomplished simply by moving the coverslip into the new medium. NsPEF treatments of cells on ITO coverslips were highly efficient, requiring about 20-fold fewer pulses than for cells in suspension. Of note, cells grown on a wrong (non-ITO) surface of the coverslip were fully shielded and could not be damaged by any number of pulses.

2.5. Buffers for nsPEF exposure and post-exposure incubation of adherent cells

For nsPEF exposure, a 1-mm cuvette was filled with a buffer containing either 2 mM Ca^{2+} or no added Ca^{2+}. Both buffers contained (in mM) 136 NaCl, 5 KCl, 2 $MgCl_2$, 10 HEPES, and 10 Glucose, and were supplemented with either 2 mM $CaCl_2$ or extra 3 mM NaCl, respectively.

For post-exposure incubation and cell imaging, we either used the same buffers, or mixed them 7:3 with an isoosmotic sucrose solution ("no Ca^{2+} + sucrose" and "2 Ca^{2+} + sucrose"). For the latter buffer, the sucrose also contained 2 mM Ca^{2+} to prevent Ca^{2+} dilution. The presence of sucrose prevented the colloid-osmotic swelling and membrane rupture of nanoporated cells [14,15].

In addition, the post-exposure incubation buffers contained 3 dyes, namely Hoechst (0.5 μg/ml), YO-PRO-1 (1 μM), and propidium (Pr) iodide (50 μg/ml). Cell-permeant Hoechst was used to label nuclei in all cells, whereas poorly permeant YO-PRO-1 and impermeant Pr served as markers of cell permeabilization. The buffers that were used during nsPEF exposure were always formulated without the dyes.

The osmolality of all buffers was at 290–310 mOsm/kg, as verified with a freezing point microosmometer (Advanced Instruments, Inc., Norwood, MA), and their pH was adjusted to 7.4. The chemicals and dyes were purchased from Sigma-Aldrich and from Life Technologies.

2.6. Experiment protocol and monitoring of permeabilization of adherent cells

Standard glass coverslips (#0 thickness, 8 mm diameter) were covered with ITO by Diamond Coatings (Halesowen, UK). For better cell

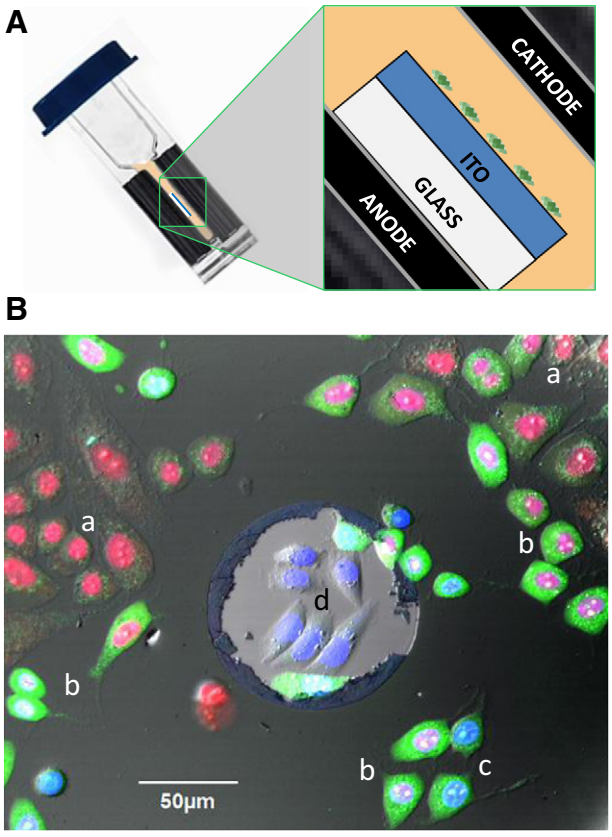

Fig. 1. Exposure of ITO-coated coverslips in electroporation cuvettes (A) and the critical role of the ITO layer in delivering the electric field to adherent cells (B). The schematic in (A) shows the position of the ITO coverslip with cells inside an electroporation cuvette (not to scale). (B): Overlaid fluorescence and DIC images of CHO cells at 2 h after nsPEF exposure (20 pulses, 300 ns duration, 20 Hz, 600 V, on ITO coverslip in a 1-mm electroporation cuvette). The cells were held in 2 mM Ca^{2+} buffer with Hoechst (blue), Yo-PRO-1 (green), and Pr (red), see Methods for details. The lighter area in the center is a random defect in ITO coating. Labels indicate: (a) dead cells with Pr-stained nuclei; (b) dying cells with Pr-stained nucleus and Yo-PRO-1 stained cytosol; (c) electropermeabilized but otherwise healthy cells with YO-PRO-1 staining of cytosol and mixed Hoechst and Yo-PRO-1 staining of the nucleus; and (d) healthy, unaffected cells displaying only Hoechst labeling of the nucleus. Note that the unaffected cells are only found within the ITO defect.

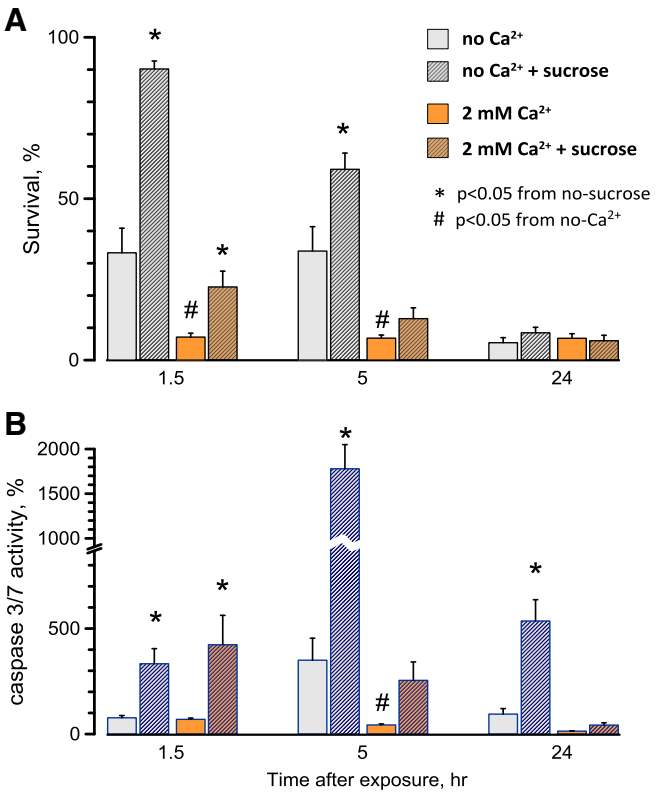

Fig. 2. Effect of extracellular Ca^{2+} and sucrose on the survival (A) and caspase 3/7 activation (B) in nanoelectroporated U937 cells. Mean values +/- s.e. for 4 independent experiments in each group. Cells were exposed in suspension in a 1-mm gap electroporation cuvette (300 pulses, 300-ns duration, 10 Hz, 700 V). The time-matched parallel control data were taken as 100%. See text for more details on exposure conditions and protocols.

adherence, the ITO surface was treated with poly-L-lysine. CHO or BPAE cells were seeded at $1–3 \times 10^3$ cells per coverslip and cultured overnight or longer in the respective growth media.

Immediately prior to the experiment, a coverslip was briefly rinsed and placed in a glass-bottomed chamber (Warner Instruments, Hamden, CT) filled with a chosen incubation buffer. The chamber was mounted on an Olympus IX81 microscope equipped with an FV1000 confocal laser scanning system (Olympus America, Center Valley, PA). Several pre-exposure images of cells were taken, and then the coverslip was moved into a 1-mm gap electroporation cuvette filled with an exposure buffer. The cuvette was kept tilted, and the coverslip was laid flat on the bottom electrode (anode), with the glass surface facing down, and the ITO surface with cells facing up into the buffer, towards the cathode (Fig. 2A). The coverslip was promptly exposed to 20 pulses of 300 ns duration, 600 V, 20 Hz from the AVTECH generator. Within the next 20–30 s, the coverslip was returned to the microscope chamber into the incubation buffer. The time lapse imaging began in 1–3 min after the exposure. In most experiments, we took one image every 30 s for 90 min.

The critical role of the ITO layer in the electroporation of adherent cells can be best appreciated from Fig. 1B, which shows cells grown on ITO with an occasional defect of the ITO coating. At 2 h after nsPEF exposure, all cells on ITO show various degrees of YO-PRO-1 and Pr uptake; many of them no longer have the cell structure and can be considered dead. The only cells that were shielded from the electric field and escaped the electroporation are those within the ITO defect (center). These cells have a healthy appearance, and labeling of their nuclei by the cell-permeant Hoechst is not quenched by either YO-PRO-1 or Pr.

Hoechst, YO-PRO-1, and Pr were excited at 405, 488, and 543 nm, and the emission was collected at 430–470 nm, 505–525 nm, and 560–660 nm, respectively. The lasers were operated in a line sequence mode to avoid the "cross-talking" of the dyes. The sensitivity of the emission detectors was tuned towards better detection of low amounts of the dye uptake, so pixel saturation with a massive uptake was expected and acceptable. The detector sensitivity was chosen in preliminary experiments and then was kept constant throughout the study. The bright field images enhanced with the differential interference contrast (DIC) were acquired concurrently.

The image stacks were quantified with MetaMorph Advanced v. 7.7.10.0 (Molecular Devices, Foster City, CA). For each of 6 tested combinations of the exposure buffer and the incubation buffer, we performed 4–9 independent experiments and analyzed up to 800 individual cells per condition. Statistical analyses included the two-tailed *t*-test and 2 × 2 contingency table/Fisher's exact test when applicable.

3. Results and discussion

3.1. Effect of Ca^{2+} on cell survival and caspase 3/7 activation

U937 cells exposed to nsPEF in the no-Ca^{2+} medium showed both the early (necrotic) and delayed cell loss (Fig. 2A), similar to the effects observed in the full growth medium [15] which contained FBS and

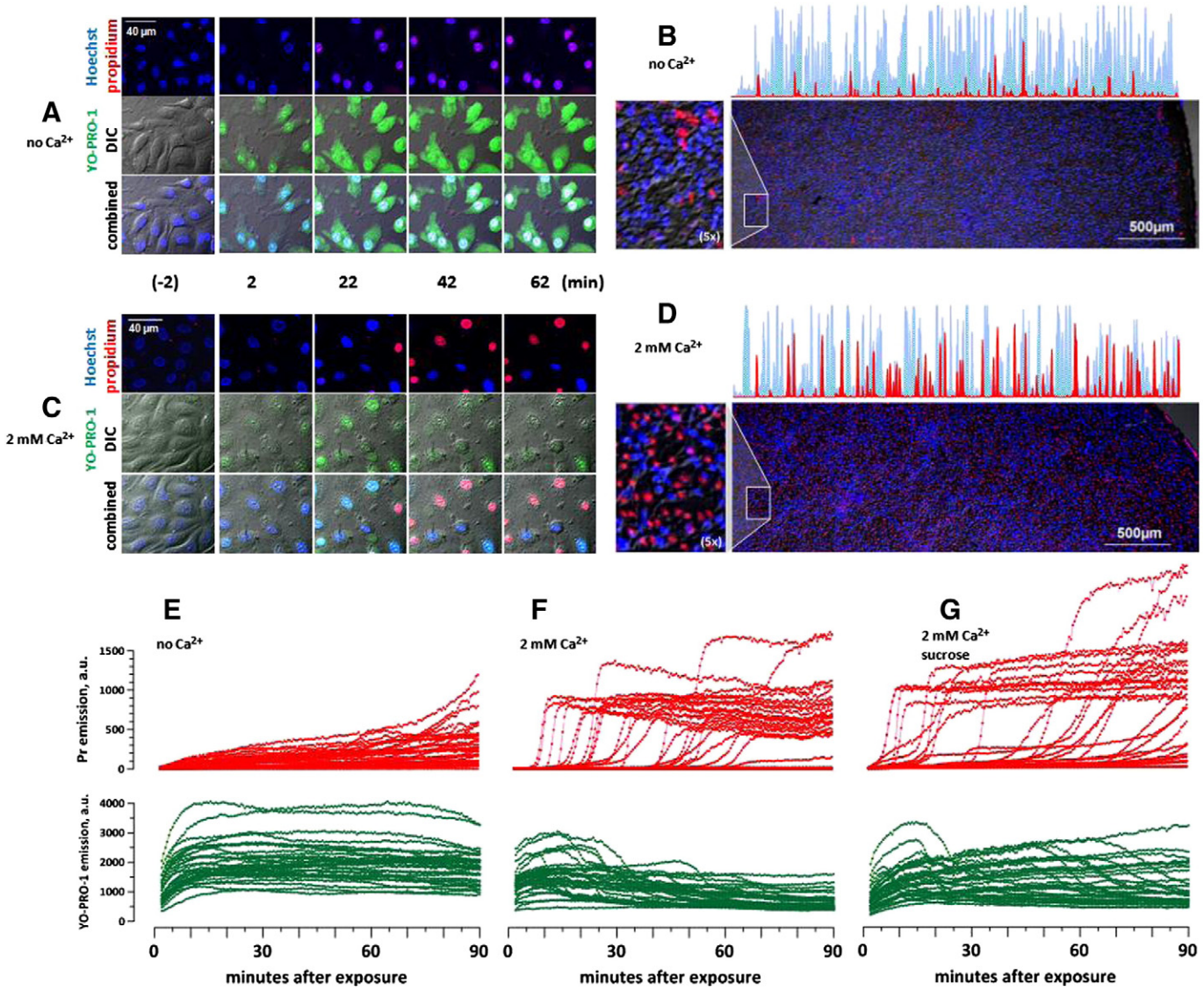

Fig. 3. Ambient Ca^{2+} determines the membrane permeability in nsPEF-treated BPAE cells. Cells were exposed to nsPEF on ITO coverslips as described in text. Both the pulsing and the incubation buffers contained no added Ca^{2+} (A, B, E) or 2 mM Ca^{2+} (C, D, F, G); in G, the incubation buffer also contained 87 mOsm/kg of sucrose. A and C: DIC and fluorescence images at selected timepoints before (−2 min) and after nsPEF exposure. In all images, Hoechst emission is shown in blue; Yo-PRO-1 is green, and Pr is red. B and D: representative low-magnification images at 90 min post nsPEF (20 pulses, 300 ns duration, 20 Hz, 600 V, on ITO coverslip in a 1-mm electroporation cuvette). Note random distribution of live (blue) and dead (red) cells over the coverslip surface and higher cell death with 2 mM Ca^{2+} (D). Also shown are selected line scans from the edge of the coverslip to its center (blue: Hoechst; red: Pr) and areas with additional 5× magnification (left). E–G: The time dynamics of Pr (top) and Yo-PRO-1 (bottom) emission in nanoporated cells. Each line in the graphs is the emission of a single, randomly chosen cell, as measured every 30 s. For clarity, the number of cells was limited to 30 per graph. Note different patterns of Pr entry without Ca^{2+} (E) and with 2 mM Ca^{2+} (F, G), and the lack of protection by sucrose (G).

0.8 mM Ca^{2+}. Somewhat higher survival in the previous study (~30% at 24 h) is consistent with the protective effect of FBS [34].

The presence of the extracellular sucrose in the no Ca^{2+} medium completely blocked the early necrosis, presumably by preventing the osmotic water uptake, cell swelling, and membrane rupture [15]. The rescued cells nonetheless died later by apoptosis ([15] and Fig. 2B), and the original idea for this study was to test if Ca^{2+} toxicity was the reason for the apoptosis. However, the experiments showed exactly the opposite effect, namely a profound increase in the early cell death and the reduced activation of caspase 3/7 when Ca^{2+} was added to the medium (Fig. 2, A,B). Over 90% of cells were dead already at 1.5 h, so there were few cells left to enter the apoptosis even if this pathway was activated.

Most surprisingly, sucrose rendered only a partial (albeit statistically significant) protection from the early necrosis in the presence of Ca^{2+}. This incomplete protection could only be explained in two ways: (a) Pores formed in the presence of 2 mM Ca^{2+} are larger than those formed in the no Ca^{2+} medium; they are permeable to sucrose, so the presence of sucrose does not inhibit the cell swelling and cannot prevent the membrane rupture, or (b) Ca^{2+} causes early necrotic cell death by a different, osmotically-independent mechanism. The next experiments were aimed at the detailed analysis of the early pore dynamics as affected by Ca^{2+} and by the inhibition of the osmotic swelling.

3.2. Cell permeabilization by nsPEF on ITO coverslips

For consistency, below we provide the data for BPAE cells, but most experiments were performed in CHO cells as well and produced essentially the same results.

Cells placed in the incubation buffer and imaged prior to nsPEF exposure expressed only Hoechst staining of the nuclei, but no YO-PRO-1 or Pr uptake (Fig. 3, A, C). Next, cells were exposed to nsPEF

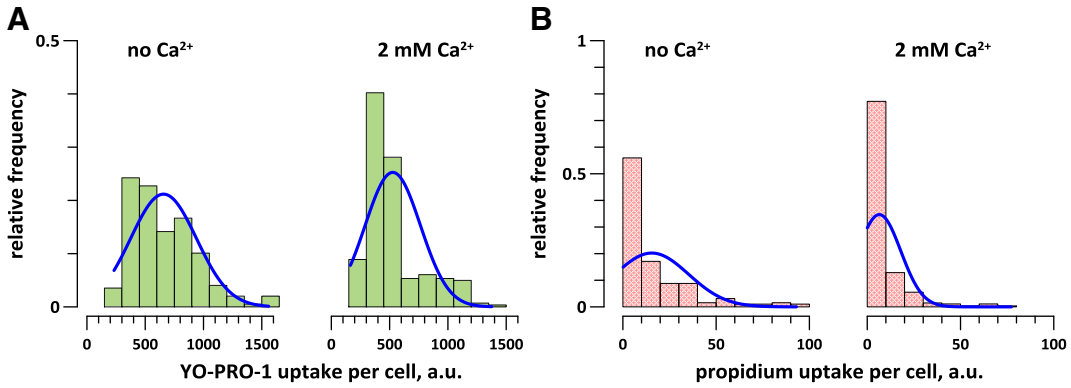

Fig. 4. High Ca^{2+} inhibits the early uptake of YO-PRO-1 (A) and Pr (B) in nanoporated BPAE cells. The uptake of the dyes was quantified at 5 min after nsPEF exposure (20 pulses, 300 ns duration, 20 Hz, 600 V, on ITO coverslip in a 1-mm electroporation cuvette). The bar height is the fraction of cells that display a particular level of Yo-PRO-1 or Pr emission (with the saturation level being at 4000 a.u. for both dyes). The exposure and bath buffer both contained either no added Ca^{2+}, or 2 mM Ca^{2+}. The effect of Ca^{2+} on dye uptake is significant at $p < 0.01$ for both dyes (200–250 cells from 4–6 independent experiments per group).

in a buffer that contained no dyes, and returned to the incubation buffer within 20–30 s. Rapid entry of YO-PRO-1 was observed immediately, indicating that nsPEF-opened membrane pores remained open (which is consistent with earlier observations of long lifetime of the nanopores [1,35–37]). At the same time, the immediate entry of Pr was rather modest or non-detectable (Figs. 3A, C, E–G and 4). The uptake of Pr typically became apparent only minutes or tens of minutes after the exposure; this late Pr uptake reflected downstream physiological changes in cells subjected to electroporation rather than direct opening of Pr-permeable pores by nsPEF.

The level of extracellular Ca^{2+} had a major impact on the membrane permeability in nanoporated cells. Cells that were incubated in the no Ca^{2+} buffer displayed a slow and gradual accumulation of Pr (Fig. 3E), also seen as a pink nuclei color from the colocalization of Hoechst and

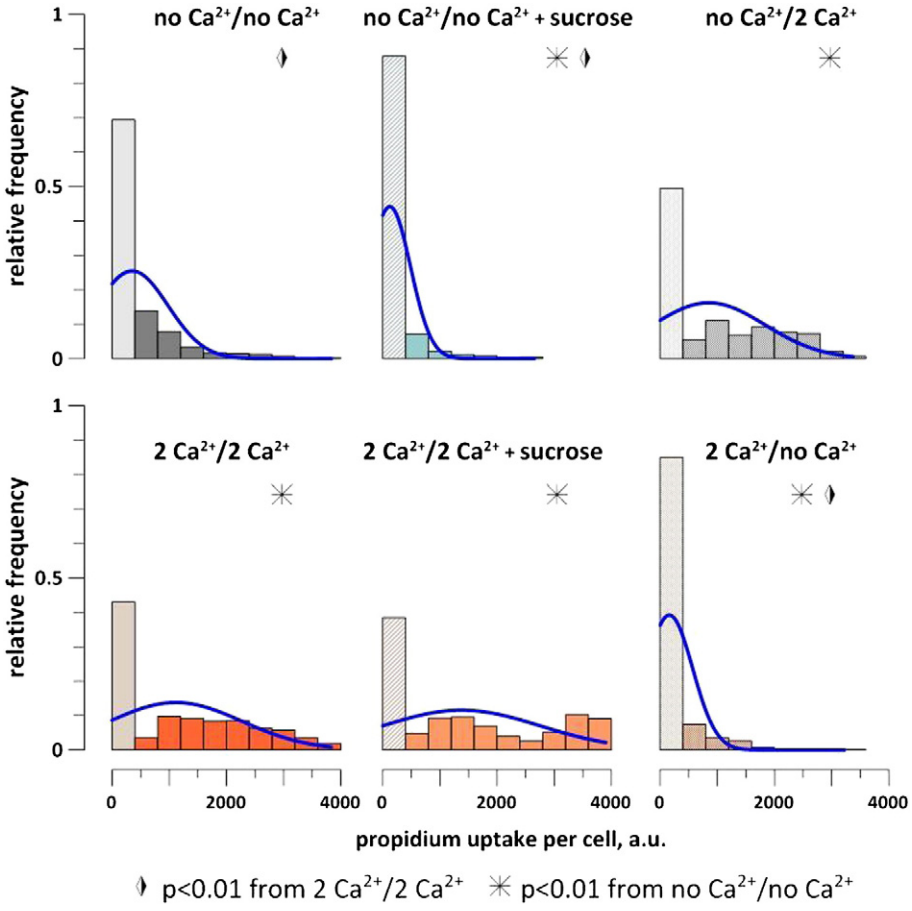

Fig. 5. The effect of bath Ca^{2+} and sucrose on Pr uptake by BPAE cells at 90 min after nsPEF (20 pulses, 300 ns duration, 20 Hz, 600 V, on ITO coverslip in a 1-mm electroporation cuvette). The legends indicate the buffer compositions (exposure/incubation). Each group includes 500–800 cells from 4–9 independent experiments. The bar height is the fraction of cells that display a particular level of Pr emission (up to the saturation at 4000 a.u.). The first bar in each chart includes cells with largely preserved membrane integrity (without Pr uptake and with less than 400 a.u. uptake). Blue curves are the normal fits. All denoted statistical differences are significant by both the two-tailed *t*-test and Fisher's exact test. See text for further details.

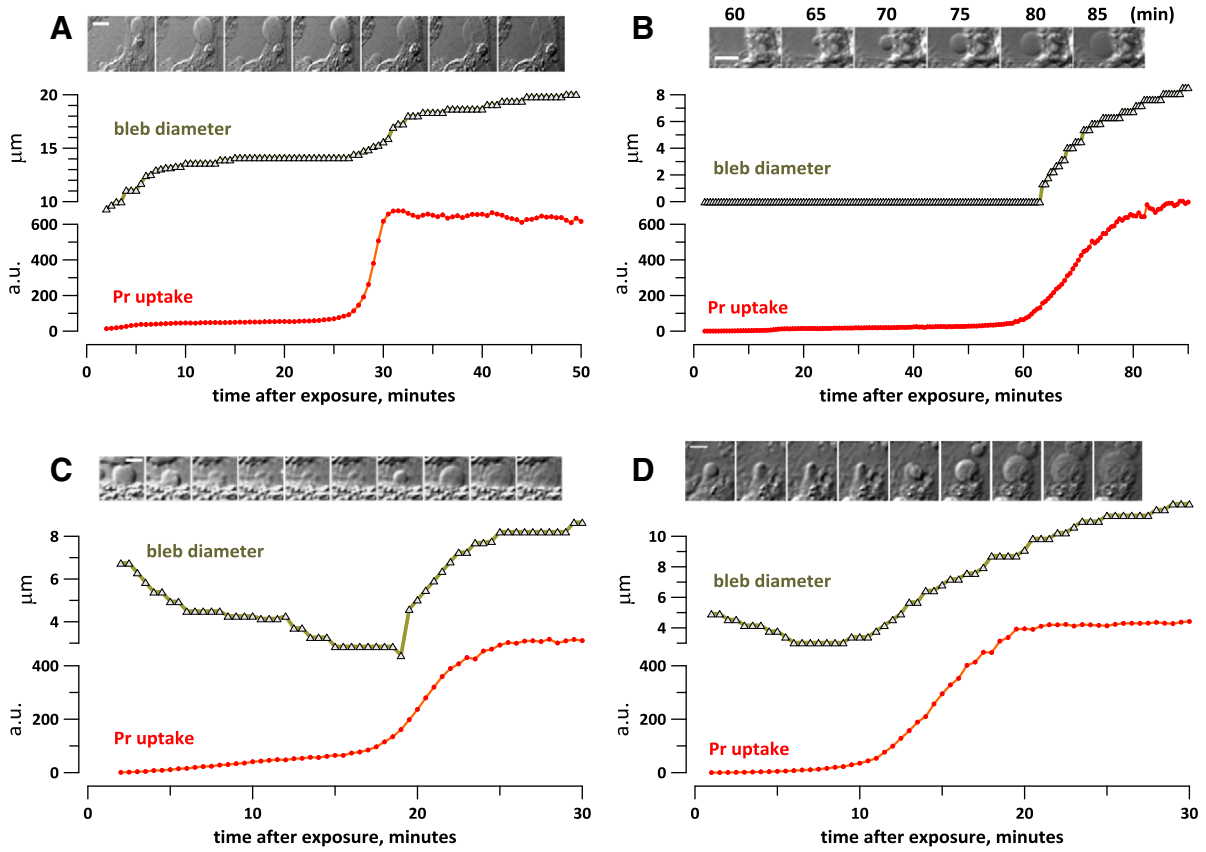

Fig. 6. Bleb growth in nanoporated cells accelerates or re-starts with the abrupt Pr uptake in BPAE (A-C) and CHO cells (D). After nsPEF exposure (20 pulses, 300 ns duration, 20 Hz, 600 V, on ITO coverslip in a 1-mm electroporation cuvette) in the 2 mM Ca^{2+} buffer, cells were incubated in the 2 mM Ca^{2+} buffer (A) or in 2 mM Ca^{2+}+sucrose buffer (B–D). The insets show DIC images of the measured blebs at the timepoints which correspond the X axis (A,C,D). In B, the time when images were taken is indicated in the legend. The calibration bar is 10 μm (A) or 5 μm (B–D).

Pr (Fig. 3A). In a sheer contrast to this pattern, cells incubated with 2 mM Ca^{2+} showed significantly less early uptake of both Yo-PRO-1 and Pr (Fig. 4), followed by an abrupt Pr inflow and quenching of both Hoechst and YO-PRO-1 (Fig. 3C, F, G). The likely mechanism of quenching was the Förster resonance energy transfer (FRET). Massive Pr uptake (at or close to the saturation level of the fluorescence detector) was accompanied by characteristic and irreversible changes in cell appearance as seen in the DIC channel (granulation, pyknosis, loss of DIC contrast and volume), and could be regarded as a sign of cell death.

By the end of a 90-min observation period after nsPEF, cell death occurrence was much higher in cells incubated with 2 mM Ca^{2+} (Fig. 3B, D). The death occurred in a seemingly random fashion, with no clear dependence on the cell density or a specific location on the coverslip surface. In isolated experiments (not shown), we observed somewhat higher survival at the edge of the coverslip, which did not impact the findings reported in this paper.

Of note, sham-exposed control samples showed no considerable Pr entry regardless of the external Ca^{2+} level or the presence of sucrose (data not shown).

3.3. Effects of Ca^{2+} on Pr uptake and cell survival are osmotically-independent

Sucrose did not change the pattern of Pr uptake in the presence of 2 mM Ca^{2+} (Fig. 3G) and did not improve the 90-min cell survival (Fig. 5). The charts in Fig. 5 summarize the Pr uptake data from over 40 individual experiments and include all cells that were in the field of vision during the time-lapse imaging (over 4000 individual cells). Cells without detectable Pr and with a low Pr expression (<10% of the maximal value) were regarded as short-term survivors. This fraction of cells (the first lighter-color bar in each chart) was significantly higher in cells incubated without Ca^{2+} than with 2 mM Ca^{2+}. The presence of sucrose blocked cell swelling and increased the survivor fraction in the no Ca^{2+} buffer, but had no protective effect with 2 mM Ca^{2+}.

Importantly, the Pr uptake and the short-term survival were determined by Ca^{2+} presence in the post-exposure incubation buffer, and much less so by Ca^{2+} in the exposure buffer (Fig. 5, right panels). When cells were exposed to nsPEF in the no Ca^{2+} buffer and then incubated with 2 mM Ca^{2+}, the Pr uptake and cell survival were similar to the effect of 2 mM Ca^{2+}. Likewise, the incubation without Ca^{2+} produced high survival levels and low Pr uptake even if the exposure was done with 2 mM Ca^{2+}. Thus, Ca^{2+} entry during and immediately after nsPEF exposure was less impactful than its entry during the subsequent incubation.

3.4. Ca^{2+} inflicts the cell death by nanopore expansion

In electroporated cells, the osmotic water uptake and cell swelling can culminate in a sudden membrane rupture, similar to overinflating a rubber balloon [15,33,38]. Admittedly these studies did not explore if there was indeed a rupture, but this mechanism fits well with both the dependence on swelling and the abrupt onset of massive Pr entry.

In this study, we observed the abrupt and massive Pr entry when the buffer contained 2 mM Ca^{2+} and swelling was presumably blocked by the sucrose (Fig. 3G). This result suggested that pores formed with 2 mM of Ca^{2+} could be large enough to admit sucrose and therefore it no longer rendered the protection from swelling. However, if the protection was actually rendered, the only alternative explanation would

be that the prolonged Ca^{2+} overload can culminate in the membrane rupture or abrupt opening of large pores even without osmotic swelling.

To discern between these two mechanisms, we monitored the size of necrotic blebs of the plasma membrane. In the presence of 2 mM Ca^{2+}, these spherical, non-retractable blebs start forming and growing immediately after the nsPEF exposure. We found that the bleb growth rate typically is high at the beginning, then stabilizes and accelerates again simultaneously with Pr entry (Fig. 6A).

When nsPEF-exposed cells are incubated in 2 mM Ca^{2+} + sucrose buffer, the bleb formation is suppressed, which is consistent with the inhibition of swelling by the presence of sucrose [14]. However, new blebs start forming and enlarging when Pr enters the cell (Fig. 6B).

Likewise, blebs which promptly formed in the exposure buffer (2 mM Ca^{2+}) start deflating upon relocation of the coverslip into the imaging chamber with 2 mM Ca^{2+} + sucrose (Fig. 6C,D). This deflation is an unambiguous manifestation of cell shrinkage and proves that membrane nanopores formed with 2 mM Ca^{2+} are not permeable to sucrose. Despite the blockage of osmotic swelling, these cells eventually experience the abrupt Pr uptake, and simultaneously the blebs switch from the deflation to inflation. The Pr molecule is larger than sucrose (about 1.5 nm vs. 1 nm [1,14]), and when pores become permeable to Pr, they became permeable to sucrose as well. Hence it comes as no surprise that sucrose cannot protect cells from swelling when many pores become permeable to Pr, and the loss of protection is manifested by restarting of the bleb growth.

The growth of blebs after the abrupt Pr entry (with or without sucrose) is an unmistakable sign that the cell membrane is not ruptured and retains only limited permeability to solutes. In contrast, a rupture of the membrane would have released the osmotic pressure, thereby eliminating the driving force for bleb growth. Thus the abrupt Pr entry is caused by pore enlargement (or perhaps formation of new pores large enough to admit Pr), but not by the membrane rupture.

4. Conclusions

Ca^{2+} overload by nanoelectroporation profoundly facilitates the early cell death and has a dual effect on membrane pores. At first, Ca^{2+} stabilizes the pores, reducing the entry of Yo-PRO-1 and reducing or abolishing the slow Pr uptake. This state is eventually replaced by an abrupt and massive Pr entry due to a sudden pore dilation, or perhaps due to a *de novo* opening of large, Pr-permeable pores. This effect is not driven by the water uptake and constitutes the final (execution) step of the osmotically-independent cell death mechanism that is caused by Ca^{2+} overload in nsPEF-treated cells. This mechanism contrasts the osmotic swelling-mediated necrotic death when nanoporated cells are incubated with lower extracellular Ca^{2+}.

Acknowledgements

The study was supported by R01GM088303 from the National Institute of General Medical Sciences and R01CA125482 from the National Cancer Institute. We also thank Dr. J. Catravas for the BPAE cells and instructions on their handling.

References

[1] A.M. Bowman, O.M. Nesin, O.N. Pakhomova, A.G. Pakhomov, Analysis of plasma membrane integrity by fluorescent detection of Tl(+) uptake, J. Membr. Biol. 236 (2010) 15–26.
[2] I. Semenov, S. Xiao, A.G. Pakhomov, Primary pathways of intracellular Ca(2+) mobilization by nanosecond pulsed electric field, Biochim. Biophys. Acta 1828 (2013) 981–989.
[3] S.J. Beebe, Y.J. Chen, N.M. Sain, K.H. Schoenbach, S. Xiao, Transient features in nanosecond pulsed electric fields differentially modulate mitochondria and viability, PLoS One 7 (2012) e51349.
[4] T.B. Napotnik, Y.H. Wu, M.A. Gundersen, D. Miklavcic, P.T. Vernier, Nanosecond electric pulses cause mitochondrial membrane permeabilization in Jurkat cells, Bioelectromagnetics 33 (2012) 257–264.
[5] A.G. Pakhomov, R. Shevin, J.A. White, J.F. Kolb, O.N. Pakhomova, R.P. Joshi, K.H. Schoenbach, Membrane permeabilization and cell damage by ultrashort electric field shocks, Arch. Biochem. Biophys. 465 (2007) 109–118.
[6] I. Semenov, S. Xiao, O.N. Pakhomova, A.G. Pakhomov, Recruitment of the intracellular Ca by ultrashort electric stimuli: the impact of pulse duration, Cell Calcium 54 (2013) 145–150.
[7] K.S. Schoenbach, B. Hargrave, R.P. Joshi, J. Kolb, C. Osgood, R. Nuccitelli, A.G. Pakhomov, J. Swanson, M. Stacey, J.A. White, S. Xiao, J. Zhang, S.J. Beebe, P.F. Blackmore, E.S. Buescher, Bioelectric effects of nanosecond pulses, IEEE Trans. Dielectr. Electr. Insul. 14 (2007) 1088–1109.
[8] J.A. White, P.F. Blackmore, K.H. Schoenbach, S.J. Beebe, Stimulation of capacitative calcium entry in HL-60 cells by nanosecond pulsed electric fields, J. Biol. Chem. 279 (2004) 22964–22972.
[9] P.T. Vernier, Y. Sun, M.T. Chen, M.A. Gundersen, G.L. Craviso, Nanosecond electric pulse-induced calcium entry into chromaffin cells, Bioelectrochemistry 73 (2008) 1–4.
[10] G.L. Craviso, S. Choe, P. Chatterjee, I. Chatterjee, P.T. Vernier, Nanosecond electric pulses: a novel stimulus for triggering Ca^{2+} influx into chromaffin cells via voltage-gated Ca^{2+} channels, Cell. Mol. Neurobiol. 30 (2010) 1259–1265.
[11] T. Berghofer, C. Eing, B. Flickinger, P. Hohenberger, L.H. Wegner, W. Frey, P. Nick, Nanosecond electric pulses trigger actin responses in plant cells, Biochem. Biophys. Res. Commun. 387 (2009) 590–595.
[12] A.G. Pakhomov, S. Xiao, O.N. Pakhomova, I. Semenov, M.A. Kuipers, B.L. Ibey, Disassembly of actin structures by nanosecond pulsed electric field is a downstream effect of cell swelling, Bioelectrochemistry (2014), http://dx.doi.org/10.1016/j.bioelechem.2014.01.004 [Epub ahead of print, pii: S1567-5394(14)00016-4].
[13] G.L. Thompson, C. Roth, G. Tolstykh, M. Kuipers, B.L. Ibey, Disruption of the actin cortex contributes to susceptibility of mammalian cells to nanosecond pulsed electric fields, Bioelectromagnetics 35 (2014) 262–272.
[14] O.M. Nesin, O.N. Pakhomova, S. Xiao, A.G. Pakhomov, Manipulation of cell volume and membrane pore comparison following single cell permeabilization with 60- and 600-ns electric pulses, Biochim. Biophys. Acta 3 (2011) 792–801.
[15] O.N. Pakhomova, B.W. Gregory, I. Semenov, A.G. Pakhomov, Two modes of cell death caused by exposure to nanosecond pulsed electric field, PLoS One 8 (2013) e70278.
[16] M.A. Rassokhin, A.G. Pakhomov, Electric field exposure triggers and guides formation of pseudopod-like blebs in U937 monocytes, J. Membr. Biol. 245 (2012) 521–529.
[17] K. Morotomi-Yano, H. Akiyama, K. Yano, Nanosecond pulsed electric fields activate AMP-activated protein kinase: implications for calcium-mediated activation of cellular signaling, Biochem. Biophys. Res. Commun. 428 (2012) 371–375.
[18] K. Morotomi-Yano, H. Akiyama, K. Yano, Nanosecond pulsed electric fields induce poly(ADP-ribose) formation and non-apoptotic cell death in HeLa S3 cells, Biochem. Biophys. Res. Commun. 438 (2013) 557–562.
[19] G.P. Tolstykh, H.T. Beier, C.C. Roth, G.L. Thompson, J.A. Payne, M.A. Kuipers, B.L. Ibey, Activation of intracellular phosphoinositide signaling after a single 600 nanosecond electric pulse, Bioelectrochemistry 94 (2013) 23–29.
[20] G.P. Tolstykh, H.T. Beier, C.C. Roth, G.L. Thompson, B.L. Ibey, 600 ns pulse electric field-induced phosphatidylinositol-bisphosphate depletion, Bioelectrochemistry (2014), http://dx.doi.org/10.1016/j.bioelechem.2014.01.006 [Epub ahead of print, pii: S1567-5394(14)00018-8].
[21] W. Ren, N.M. Sain, S.J. Beebe, Nanosecond pulsed electric fields (nsPEFs) activate intrinsic caspase-dependent and caspase-independent cell death in Jurkat cells, Biochem. Biophys. Res. Commun. 421 (2012) 808–812.
[22] X. Chen, J. Zhuang, J.F. Kolb, K.H. Schoenbach, S.J. Beebe, Long term survival of mice with hepatocellular carcinoma after pulse power ablation with nanosecond pulsed electric fields, Technol. Cancer Res. Treat. 11 (2012) 83–93.
[23] R. Nuccitelli, J. Huynh, K. Lui, R. Wood, M. Kreis, B. Athos, P. Nuccitelli, Nanoelectroablation of human pancreatic carcinoma in a murine xenograft model without recurrence, Int. J. Cancer 132 (2013) 1933–1939.
[24] R. Nuccitelli, K. Tran, K. Lui, J. Huynh, B. Athos, M. Kreis, P. Nuccitelli, E.C. De Fabo, Non-thermal nanoelectroablation of UV-induced murine melanomas stimulates an immune response, Pigment Cell Melanoma Res 25 (2012) 618–629.
[25] D. Yin, W.G. Yang, J. Weissberg, C.B. Goff, W. Chen, Y. Kuwayama, A. Leiter, H. Xing, A. Meixel, D. Gaut, F. Kirkbir, D. Sawcer, P.T. Vernier, J.W. Said, M.A. Gundersen, H.P. Koeffler, Cutaneous papilloma and squamous cell carcinoma therapy utilizing nanosecond pulsed electric fields (nsPEF), PLoS One 7 (2012) e43891.
[26] M. Breton, L.M. Mir, Microsecond and nanosecond electric pulses in cancer treatments, Bioelectromagnetics 33 (2012) 106–123.
[27] B. Zhivotovsky, S. Orrenius, Calcium and cell death mechanisms: a perspective from the cell death community, Cell Calcium 50 (2011) 211–221.
[28] R. Nuccitelli, K. Lui, M. Kreis, B. Athos, P. Nuccitelli, Nanosecond pulsed electric field stimulation of reactive oxygen species in human pancreatic cancer cells is Ca(2+)-dependent, Biochem. Biophys. Res. Commun. 435 (2013) 580–585.
[29] G.L. Craviso, S. Choe, I. Chatterjee, P.T. Vernier, Modulation of intracellular Ca(2+) levels in chromaffin cells by nanoelectropulses, Bioelectrochemistry 87 (2012) 244–252.
[30] A.G. Pakhomov, I. Semenov, S. Xiao, O.N. Pakhomova, B. Gregory, K.H. Schoenbach, J.C. Ullery, H.T. Beier, S.R. Rajulapati, B.L. Ibey, Cancellation of cellular responses to nanoelectroporation by reversing the stimulus polarity, Cell. Mol. Life Sci. (2014) [Epub ahead of print].
[31] S.K. Frandsen, H. Gissel, P. Hojman, T. Tramm, J. Eriksen, J. Gehl, Direct therapeutic applications of calcium electroporation to effectively induce tumor necrosis, Cancer Res. 72 (2012) 1336–1341.

[32] B.L. Ibey, C.C. Roth, A.G. Pakhomov, J.A. Bernhard, G.J. Wilmink, O.N. Pakhomova, Dose-dependent thresholds of 10-ns electric pulse induced plasma membrane disruption and cytotoxicity in multiple cell lines, PLoS One 6 (2011) e15642.
[33] O.N. Pakhomova, B.W. Gregory, V.A. Khorokhorina, A.M. Bowman, S. Xiao, A.G. Pakhomov, Electroporation-induced electrosensitization, PLoS One 6 (2011) e17100.
[34] C. Delteil, J. Teissie, M.P. Rols, Effect of serum on in vitro electrically mediated gene delivery and expression in mammalian cells, Biochim. Biophys. Acta 1467 (2000) 362–368.
[35] A.G. Pakhomov, A.M. Bowman, B.L. Ibey, F.M. Andre, O.N. Pakhomova, K.H. Schoenbach, Lipid nanopores can form a stable, ion channel-like conduction pathway in cell membrane, Biochem. Biophys. Res. Commun. 385 (2009) 181–186.
[36] A.G. Pakhomov, O.N. Pakhomova, Nanopores: a distinct transmembrane passageway in electroporated cells, in: A.G. Pakhomov, D. Miklavcic, M.S. Markov (Eds.), Advanced Electroporation Techniques in Biology in Medicine, CRC Press, Boca Raton, 2010, pp. 178–194.
[37] A.G. Pakhomov, J.F. Kolb, J.A. White, R.P. Joshi, S. Xiao, K.H. Schoenbach, Long-lasting plasma membrane permeabilization in mammalian cells by nanosecond pulsed electric field (nsPEF), Bioelectromagnetics 28 (2007) 655–663.
[38] K. Kinosita Jr., T.T. Tsong, Hemolysis of human erythrocytes by transient electric field, Proc. Natl. Acad. Sci. U. S. A. 74 (1977) 1923–1927.